Unité de Biophysique Cellulaire et moléculaire[1], Centre de Recherches du Service de Santé des Armées, La Tranche, Laboratoire de Chimie Thérapeutique[2], Faculté de Pharmacie de Tours, Centre d'Etudes Nucléaires[3], Grenoble and Institut de Biologie Structurale[4], Grenoble, France

Modulation of intercalating properties of pyrido[1,2-*e*]purins via side-chain modifications: NMR and MD studies

J. C. Debouzy[1], V. Dabouis[1] , S. Crouzy[3,] , C. Bachelet[1], A. Favier[4], A. Peinnequin[1] and A. Gueiffier[2]

Two pyrido[1,2-*e*]purins with different side chain lengths have been synthesized to test their ability to intercalate inside DNA. The interactions of these drugs with synthetic oligodeoxy nucleotide $d(CGATCG)_2$ have been studied with ^1H and ^{31}P NMR spectroscopy experiments. Molecule **1**, rather amphiphilic (Log(P) = 1.3, due to its hydroxypropyl side chain) can intercalate GC sites of the mini helix, under a fast exchange mechanism and a 2 : 1 stoechiometry. The presence of a six methylen side chain in **2** (hydroxyhexyl side chain) is responsible for a relatively poor solubility of this molecule in water (log P = 2.3). Binding, rather than intercalation, of **2** to the external GC pairs is observed, severely limited by the formation of aggregates. Models for the intercalation of **1**, are proposed using energy minimizations and Molecular Dynamics (MD) calculations subject to restraints from experimental nOe connectivities. Simulations and experiments both indicate fast exchange of **1** in its intercalation site.

1. Introduction

Several food pyrolysis products are well-identified as potential carcinogens [1, 2] via a direct interaction with DNA, generally by intercalation or strand breaks. Among them, Glu-P1, (2-amino-6-methyl dipyrido[1,2-*a*:3′,2′-*d*]-imidazole, the pyrolysis product of glutamin) was the least mutagenic while inducing the maximum DNA strand breaks: this structure was used as a starting point to form nitrogen bridged structures [3] close to some anticancer imidazo[1,2-*a*]azines [4–6]. These first molecules presented reduced mutagenic properties while keeping their affinity for DNA. However, their hydrophobicity, limiting their ability to cross biological barriers, was a severe restriction to their use. Therefore, amphiphilic derivatives were synthesized to obtain enhanced interactions with both membranes and oligonucleotides (see nomenclature in the result section). The dramatic differences in the biological anticancer activity [7] of these drugs, despite an identical basic pyridopurin core, motivated a deeper investigation of their properties. Crucial points in drug design are their possibility of transport in biological systems-fluids and membranes-, and obviously, their interaction with the molecular target, here DNA. The amphiphilic properties of these molecules, and also the interactions of **1** with membranes were demonstrated in our previous work [8, 9]. Their interactions with the oligonucleotide $d(CGATCG)_2$ are the subject of the present paper.

2. Investigations and results

2.1. Structure

The two derivatives were synthesized from 4-chloro-pyrido[1,2-*e*]purine **A**, as described elsewhere [7].

2.2. Interactions with oligonucleotide d(CGATCG)$_2$

The interactions of **1**, and **2** with $d(CGATCG)_2$ (nomenclature $d(C1G2A3T4C5G6)_2$ were investigated using NMR spectroscopy on the different building blocks of the DNA fragment, i.e by recording ^1H NMR spectra of the imino-protons engaged in hydrogen bonds in the duplex, the non labile protons of the bases and the sugar groups and also by recording ^{31}P NMR spectra of the inter residue phosphate groups.

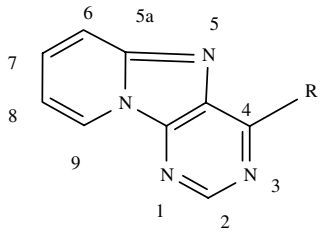

A (R=Cl)
1 R = $-NH(CH_2)_4OH$,
2 R = $-NH(CH_2)_6OH$

2.2.1. Observation of the exchangeable protons of d(CGATCG)$_2$ in H$_2$O

The downfield part of the ^1H NMR spectrum of $d(CGATCG)_2$ recorded at 277 K is shown in Fig. 1. As previously described [10], the three expected resonances of bonded imino protons were identified as follows:

– the central broad resonance (13 ppm) that vanishes with increasing temperature was attributed to external GC

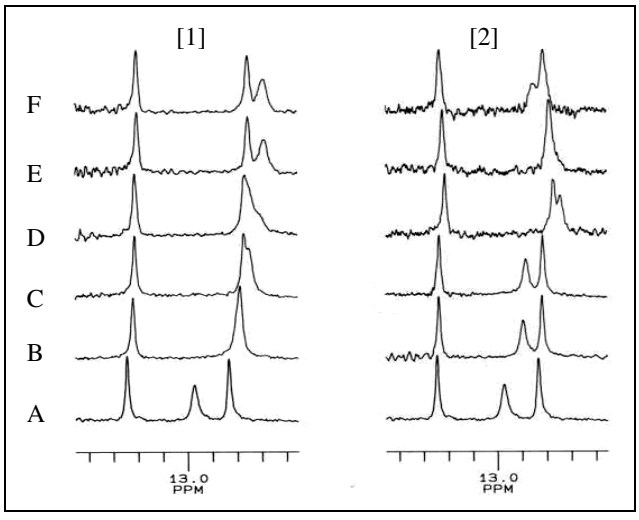

Fig. 1: Imino part of ^1H NMR spectra of pure $d(CGATCG)_2$ (4 mM, 277 K, H2O/D2O90/10, bottom traces) and in the presence of **1** (left) or **2** with drug/$d(CGATCG)_2$. molar ratios of: A: 0, B: 0.25, C: 0.5, D: 0.8, E: 1, F: 2. (from bottom to top)

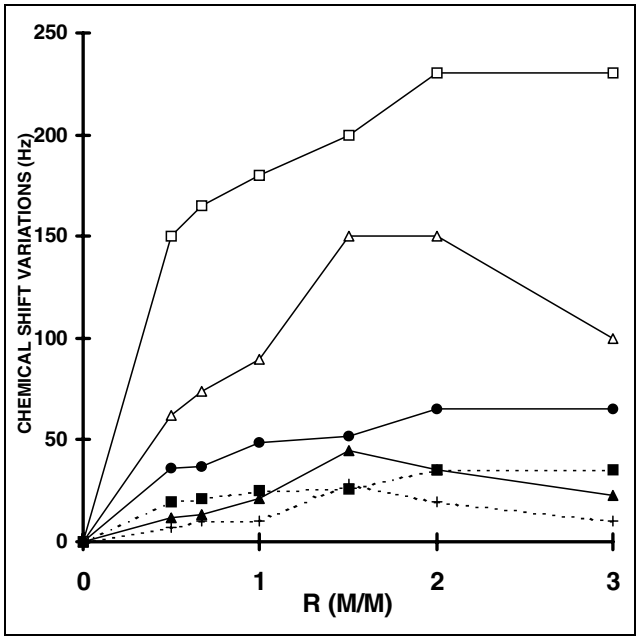

Fig. 2: ^{1}H NMR chemical shift variations (Hz) of C1G6, C2G5 and A3T4 imino protons of d(CGATCG)$_2$ respectively, in the presence of **1** (□, ●, ¦), **2** (△, ▲, +) as a function of drug/d(CGATCG)$_2$ ratio R(W/W), at 277 K, using the jump/return sequence starting from 4 mM d(CGATCG)$_2$. 4 mM, 277 K, H_2O/D_2O, (90/10, v/v)

pairs. Irradiation of the resonance located around 13.5 ppm induces a nOe with the H_2 proton of 3A; this resonance was attibuted to the imino proton A3T4/T4A3. The other resonance (12.7 ppm) was attributed to G2C5/C5G2. As described before, intercalating drugs, groove binders and non specific outside binders can be easily identified by the observation of the chemical shift and linewidth variations of imino protons. Successive spectra of d(CGATCG)$_2$ were then recorded in the presence of increasing amounts of **1** and **2**, as shown from bottom to top in Fig. 1. The chemical shift variations, presented in Fig. 2, clearly show that addition of **1** gives rise to large chemical shift variations. All imino resonances continuously upfield shift upon drug addition, while no new peak is detected even at 2 °C, indicating a fast exchange between free and bound species [11]. As described elsewhere, such an evolution is generally considered as suggestive of intercalation [12]. It clearly appears that the imino protons of the GC pairs are significantly more shifted than those of the AT pairs (200 Hz (C1G6), 50 Hz (C5G2) against 25 Hz (AT) for **1**/d(CGATCG)$_2$ = 1, M/M), indicating a preferential GC intercalation. Moreover, after similar experiments performed under constant total concentration ([drug] + [dCGATCG] = 4 mM), A Job-plot [13] of the chemical shift variations weighted by the concentration as a function of the molar fraction (F), (not shown) was built from the chemical shift variations of GC pairs. It shows a maximum when the stoichiometry is reached, here F = 0.5, i.e. when 2 molecules of **1** can intercalate the duplex d(CGATCG)$_2$.

Addition of **2** did not lead to similar observations (Fig. 1, right column): Up to equimolar **2**/d(CGATCG)$_2$ ratio the chemical shift variations of imino protons were similar to those observed with **1** while of lower magnitude (150 Hz for C1G6, 45 Hz for C5G2 and 15 Hz for A3T3). However, an opposite evolution of all chemical shifts was found after further addition of **2** (95 Hz, C1G6; 23 Hz, C5G2; 10 Hz, A3T3 for 3/1 **2**/d(CGATCG)$_2$ ratio). It should be noticed that the starting concentration used for d(CGATCG)$_2$ was 3 mM, and that **2** is not soluble in water at such concentrations, i.e. those inducing the most important chemical shift variations. This is an indication that **2** is not exclusively in the bulk, but partly bound to the oligonucleotide. Increasing the amount of **2** leads to formation of precipitates and a loss of **2** ^{1}H-resonance intensities. This indicates that, rather than a simple saturation of a poorly soluble molecule, a competition with the binding mechanism has also occured toward agregate/micelles formation, in accord with our previous work [8].

From the relative broadening and the maximum shift of imino proton lines observed in the presence of **1**, the lifetime of the bound state can be calculated following Feigon and Coll [12]: they show that the maximum chemical shift difference δm (Hz) observed in the presence of the drug and the lifetime, in the conditions of fast exchange are related by:

$$\delta m = 1/\pi^* t \qquad (1)$$

where t is expressed in seconds. In the present case, δm was measured for C5G around 70 Hz for both **1** and **2** giving a value for $t \approx 4.5$ ms. The conditions of fast exchange were satisfied, since no significant line broadening was found after drug addition (18 Hz at drug saturation against 14 Hz for d(CGATCG)$_2$ alone) or after cooling the sample to 2 °C.

On the other hand, a linewidth of 30 Hz measured on pure d(CGATCG)$_2$ for the C1G6 resonance is indicative of the easy binding/unbinding of external pairs. (This exchange broadening leads to a complete vanishment of C1G6 resonance at temperatures exceeding 10 °C). The addition of the drugs **1** led – beside the dramatic chemical shift variations – to supplementary broadening of 35 Hz at saturation. This led us to use the relation proposed by Feigon in the case of intermediate exchanges,

$$\Delta\nu = 1/\pi^* t \qquad (2)$$

that provided another estimation for t = 9 ms. This result shows that the life time of the bound state for C1G6 pairs is in the same range as that for C5G2 pairs.

2.2.2. Non-exchangeable protons of (CGATCG)$_2$

d(CGATCG)$_2$ proton assignment was performed using HOHAHA, COSY and NOESY experiments according to previous works [11, 12, 14]. The proton chemical shifts of d(CGATCG)$_2$ alone and in the presence of **1**, **2** are listed in Table 1. Beside the aromatic region, the H1′ region of the spectrum (see Fig. 3, top) gives information about the sugar puckering in the oligomer. At 277 K, the different coupling patterns with H2′/″ provide similar triplets, typical of a predominant South conformation. The presence of a B structure was also confirmed by the relative intensities of NOEs between $H^{6/8}$ and H2′/″ protons ($H^{2'}(i)-H^{6/8}(i) > H^{2''}-H6/8(i+1) > H^{2'}(i)-H^{6/8}(i+1)$). These anomeric resonances were not significantly modified in their coupling patterns after drug addition. However, both Table 1 and Fig. 3 (bottom) show that, in the presence of **1**, several highfield chemical shift variations, even if relatively weak, are measured on G6, C1 and C6 sugar resonances, while others are only slightly displaced.

On the other hand, the addition of **2**, induced no significant chemical shift and almost no variation of coupling constants on ^{1}H NMR spectra. The same observations apply for base resonances (see $1C^5$ (proton 5 of cytosine 1) and $5C^5$ doublets in Fig. 3): chemical shift variations are

Table 1: Chemical shifts and chemical shift variations of d(CGATCG)$_2$, alone and in the presence of [1] and [2] at 296 K (molar ratios duplex/drug of 1). (X), not clearly resolved

H		H6/8	H2/5	H1′	H2′	H2″	H3′	H4′	H5′/″
1C	Free	7.64	5.87	5.77	2.40	1.86	4.70	4.10	3.73
	[1]	−16	−7	−5	−1	0	−5	0	0
	[2]	−4	−2	0	0	0	−1	0	0
2G	Free	8.02	–	5.60	2.79	2.83	5.03	4.36	44.1
	[1]	0	0	−12	−3	0	0	0	0
3A	Free	−8.33	7.99	6.36	2.76	3.00	5.06	4.52	4.3
4T	Free	7.24	1.45	6.00	2.05	2.47	4.87	4.19	4.29
	[1]	−6	0	−5	0	0	0	0	0
5C	Free	7.52	5.70	5.82	2.04	2.42	4.85	4.18	4.10
	[1]	−8	0	−20	0	0	0	0	0
6G	Free	8.01	–	6.21	2.66	2.45	4.70	4.21	4.14
	[1]	−8	0	−20	0	0	0	0	X
	[2]	0	0	−5	0	0	0	0	0

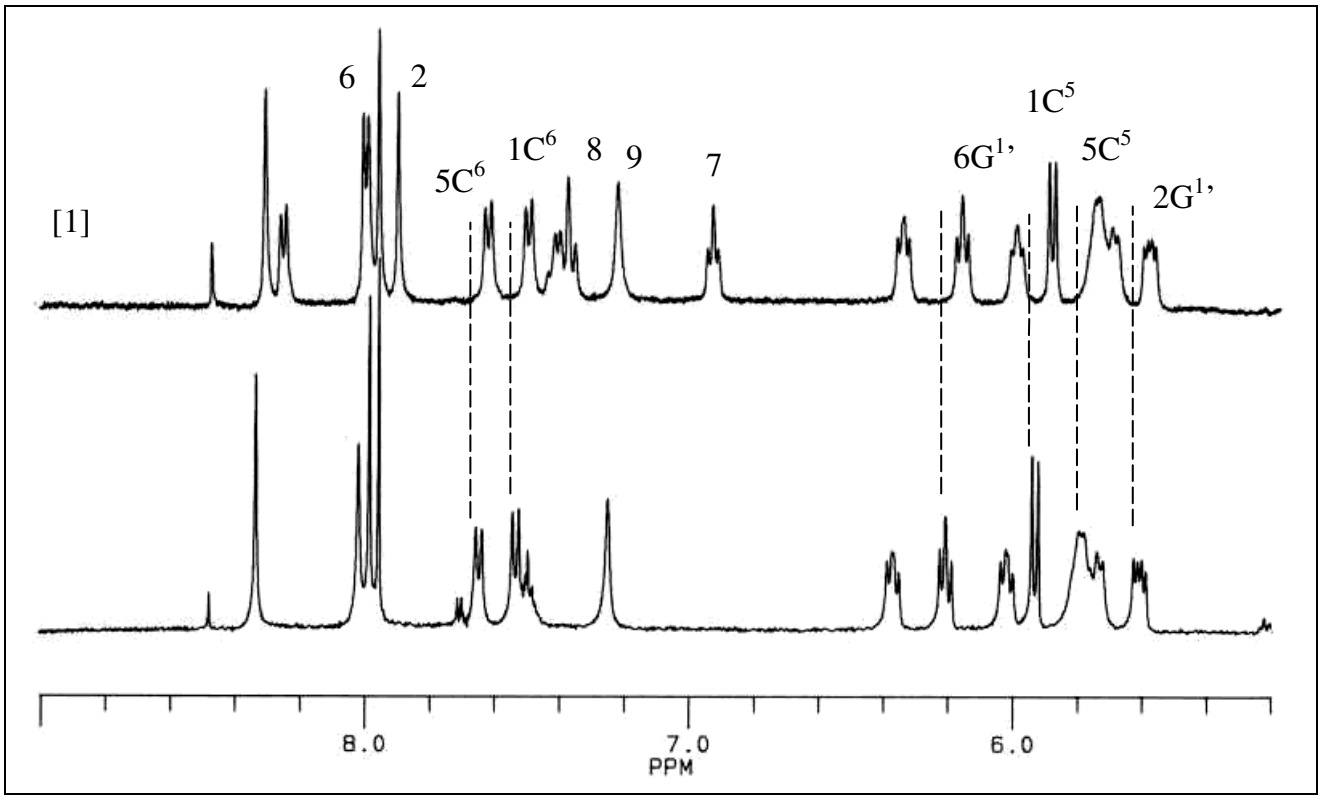

Fig. 3: Partial ^{1}H NMR spectrum of pure d(CGATCG)$_2$, (4 mM, 277 K, D_2O, bottom); B) equimolar **1**/d(CGATCG)$_2$, preparation (top). Proton labelling follows: base number, base initial, proton number

measured on 1C^5, 5C^5 and 6G$^{1'}$ resonances in the presence of **1**, while these modifications are absent for **2**.

^{31}P NMR spectroscopy was then used to observe the influence of the binding of the drug on phosphorus resonances.

^{31}P NMR spectroscopy has been extensively used to probe DNA intercalation since this mode of binding generally leads to downfield shifts of the ^{31}P NMR signal around the site of intercalation [14]. The spectrum of native d(CGATCG)$_2$ (283 K) presented on the top trace of Fig. 4 shows five resonances that were attributed using data and references from the literature [15] and HMQC control experiments. This spectrum is similar to that recorded in the presence of **2**, indicating the absence of interaction of the drug at the phosphorus level of the oligonucleotide. In the case of **[1],** most of the ^{31}P resonances are also unaffected by the presence of the drug. However, the P_I line (see nomenclature in Fig. 4) is clearly downfield shifted, as reported in Table 2.

Minor chemical shift variations were also detected for P_V resonances.

Finally nOesy experiments were undertaken in order to detect the spatial connectivities generally observed in the case of binding of a drug to DNA.

Table 2: Chemical shifts (ppm) and chemical shift variations of ^{31}P NMR resonances of d(CGATCG)$_2$, in the presence of 1, 2 for equimolar ratios

(Δδ, Hz)/P	I	II	III	IV	V
0, δ (ppm)	0.815	0.81	0.52	0.64	1.05
1 (Hz)	10	1	1	0	2
2 (Hz)	2	0	0	1	2

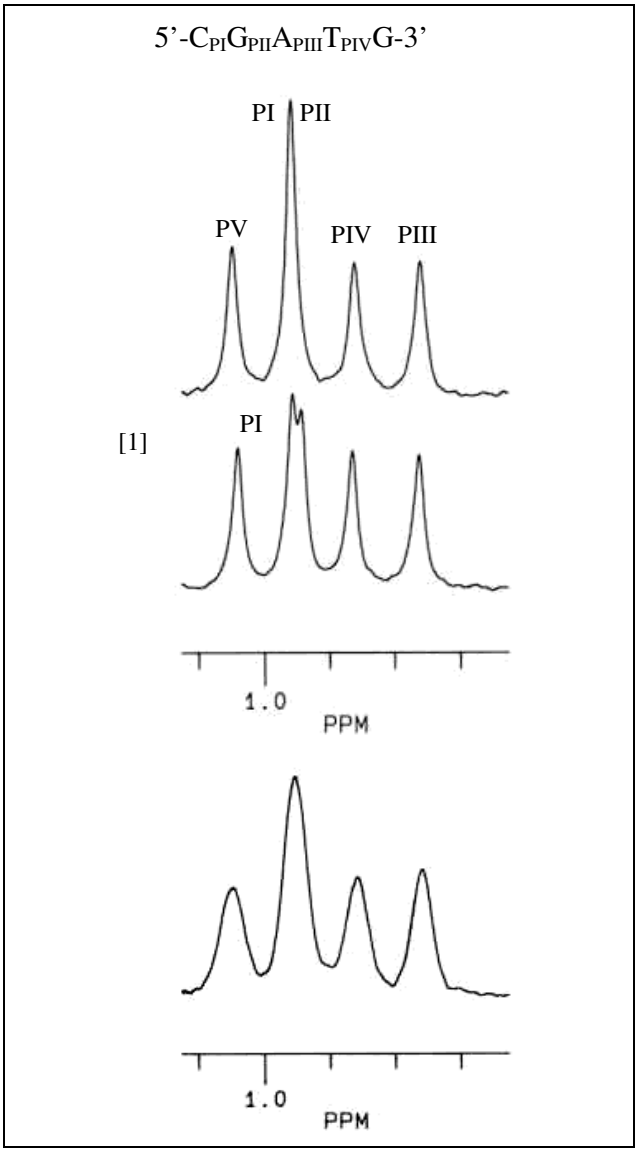

Fig. 4: ^{31}P NMR spectra of pure d(CGATCG)$_2$: (296 K, 4 mM, top trace), and in the presence of equimolar **1** (bottom): phosphorus nomenclature is presented on the top of the figure

2.2.3. NOESY experiments

The lowfield part of the NOESY map (mixing time of 400 ms) recorded on **1**/d(CGATCG)$_2$ preparation (2/1, M/M) is presented in Fig. 5. Shorter mixing times (from 70 to 250 ms) experiments were also done to avoid spin diffusion and also allow peak integration. Apart from intramolecular connectivities, used for sequential attribution of d(CGATCG)$_2$, no correlation was found at short mixing times for **2**/d(CGATCG)$_2$ systems while only weak cross peaks were observed for both **1**/d(CGATCG)$_2$ preparations with 2G$^{1'}$ and 1C$^{5'}$ protons, as shown in Table 3. Longer mixing times (0.3–0.5 s) provided the supplementary correlations for **1** containing systems, that were used for molecular modeling calculations. Most of these cross peaks revealed vicinities between the heterocycle part of **1** and the C1G2 and also C5G6 regions of the duplex whereas no intermolecular connectivity was found with the A3T4 region. Weak correlations were also detected for the terminal methylen groups of the chain and the 6G$^{1'}$ resonance.

These connectivities were used for molecular modeling calculations presented in the next section.

Table 3: NOESY connectivities

1: H					2: H
2	5C1′	5C2′/″	5C6	2′	
6	1C5	5C5			
7	1C5 1C6*	2G1′	1C3′		1C5
8	1C5 1C6	2G1′	6G1′*		
9	2G1′*	6G5′*			
1′	6G8*		6G1′*		
2′	1C5	5C5	6G1′		
6′					6G1′

* only detected for 400 ms mixing times

2.3. Molecular modeling

The ab-initio optimized geometry of **1** is shown in Fig. 6. The molecule is planar up to carbon C1′ of the tail. Characteristic angles and dihedrals are listed in Table 4.

A hydrogen bond (distance 1.95 Å) between the hydroxy hydrogen and nitrogen N5 stabilizes the molecule.

Energies obtained after minimization to a final gradient of 0.01 kcal/mol/Å^2 both before and after MD stage a) with position and distance restraints are reported in Table 5, for the 4 interaction models, in vacuum.

Model II satisfies most but not all of the experimental restraints: nOes between H6 and 5C^5 (6.4 Å), H7–2G$^{1'}$ (5.3 Å) H2′–6G$^{1'}$ (7.6 Å), H2′–5C^5 (5.7 Å) and H2′–1C^5 (6.5 Å) are not satisfied. Model IV is the only one that satisfies the nOe restraint between H6 and 5C^5. Models I, II and IV give NOE restraint energies more than twice that obtained for model II. Total energies are similar between all models with a minimum obtained for model II which seems in best agreement with experimental distances.

From these primary "in vacuo" results, it appears that an exchange between at least two intercalation models is necessary to account for all the observed nOes. A more realistic study was necessary to shed some light on the stability of each intercalation model in its solvent environment.

Table 4: Characteristic angles

Atoms	Angle (degrees)
C4–NH–C1′	127.1
NH–C1′–C2′	112.9
C1′–C2′–C3′	113.4
C2′–C3′–C4′	114.3
C3′–C4′–OH	113.4
C4–NH–C1′–C2′	85.6
NH –C1′–C2′–C3′	–172.5
C1′–C2′–C3′–C4′	87.1
C2′–C3′–C4′–OH	63.7

Table 5: Energies obtained in vacuum

	E_{Total} (before a) kcal/mol	E_{Noe} (before. a) kcal/mol	E_{Total} (after a) kcal/mol	E_{NOe} (after a) kcal/mol
Model I	–2302	42.5	–2480	38.8
Model II	–2302	20.4	–2489	17.6
Model III	–2288	41.6	–2464	35.3
Model IV	–2216	73.0	–2441	43.2

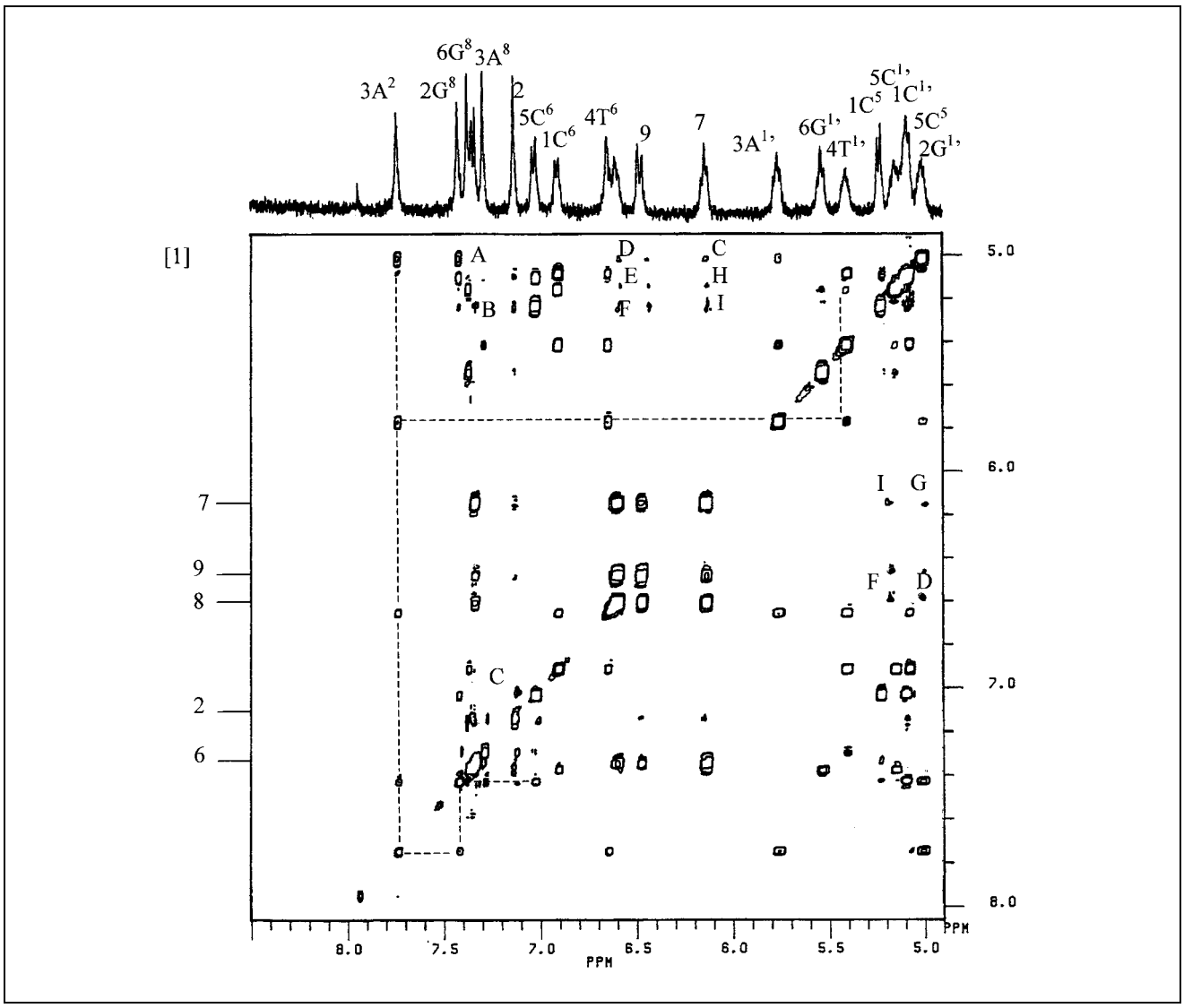

Fig. 5: Lowfield part of the NOESY map recorded on a **1**-d(CGATCG)$_2$ sample (2/1 M/M, 280 K, mixing time of 400 ms). Dashed lines represent some connectivities used for sequential attribution. Intermolecular connectivities: A) 6-5C5, B) 6-1C5, C) 2-5C6 D) 8/9-2G1′, E)8/9-5C5, F) 8/9-1C5, G) 7-2G1′, H) 7-1C1′, I)7-1C5

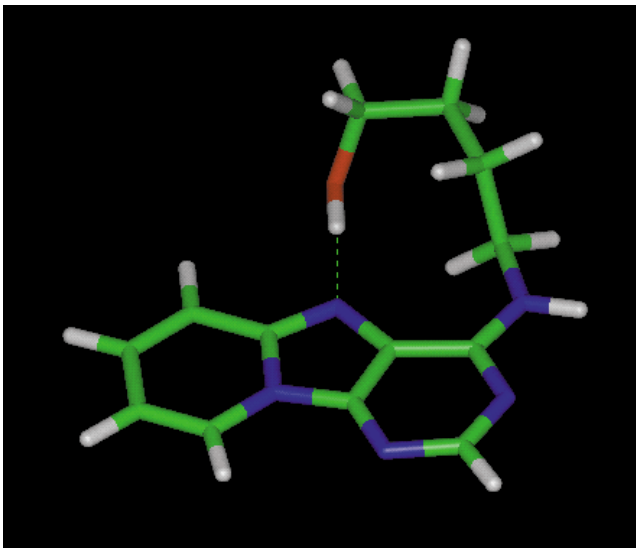

Fig. 6: Ab-initio optimized geometry of **1** The stabilizing hydrogen bond between the hydroxyl hydrogen and N5 is indicated

Energies obtained after minimization to a final gradient of 0.01 kcal/mol/Å^2 both before and after MD stage a) with position and distance restraints are reported in Table 6, for the 4 interaction models, in the presence of solvent.

Clearly, similarly to the previous "in vacuum" results, model II corresponding to an insertion of molecule **1** in the major groove of DNA, is the model that best agrees with the NMR data.

Average potential energies (and root mean square deviations) obtained during MD stages a) to c) in the presence of solvent are listed in Table 7 for the 4 intercalation models. Average harmonic and nOe distance restraint energies are also listed for stage a).

Model II presents the lowest average potential energy during stage a) in which the DNA fragment is artificially sta-

Table 6: Energies obtained in the presence of solvent

	E_{Total} (before a)	E_{Noe} (before a)	E_{Total} (after a)	E_{NOe} (after a)
Model I	−27639	37.3	−27757	34.4
Model II	−27673	18.3	−27844	19.1
Model III	−27657	37.0	−27800	33.8
Model IV	−27573	47.3	−27798	19.8

Table 7: Average potential energies

Protocol	Model			
	I	II	III	IV
a)	−22545 (67)	−22598 (62)	−22572 (65)	−22549 (63)
$a)_{HARM}$	12.5	9.1	13.1	21.2
$a)_{NOE}$	37.3	21.0	36.6	25.3
b)	−22621 (66)	−22631 (63)	−22625 (62)	−22625 (62)
c)	−22640 (72)	−22612 (65)	−22624 (66)	−22638 (60)

bilized by harmonic restraints on the position of its heavy atoms and distance restraints to keep proper Watson-Crick pairing of the bases. Model II also leads to the lowest average harmonic and nOe distance restraint energies during this stage. (The important H2-H2′ intramolecular nOe, for instance, is satisfied with a calculated average distance of 4.4 Å). The same result applies when the experimental nOe restraints are removed (stage b), while still keeping the Watson-Crick pair distance restraints. The corresponding average structure of model II is shown in Fig. 7. The colour range from blue to red reproduces the average root mean square deviations of the atoms from the average structure from 0.5 to 2.5 Å. (Water molecules and ions have been deleted for clarity). Clearly, the tail of the drug and CG external DNA base pairs present the largest fluctuations consistent with the NMR results.

When the DNA fragment is left completely free to move, (stage c), model II becomes less stable than the other models (higher potential energy). This can be explained by a too short simulation time or more likely, by a rupture of the hydrogen bonds responsible for the pairing of the external C-G bases.

In conclusion, an insertion of **1** between the CG bases in the major groove of the oligodeoxy nucleotide $d(CGATCG)_2$ with N5 atom facing C1-G2 is the model that best satisfies the ^1H NMR spectroscopy distance restraints while keeping a perfect pairing of these external bases.

3. Discussion

The two derivatives studied in the present paper were synthesized from the basic pyridopurin structure in order to obtain anticancer activity, following basic principles: first, enhance biodisponibility by increasing the overall solubility in water and second enhance intercalating properties. To meet the first criterion, obtain amphiphilic properties so as to be able to reach the intracellular target (i.e. DNA) via membrane transport, side chains of different

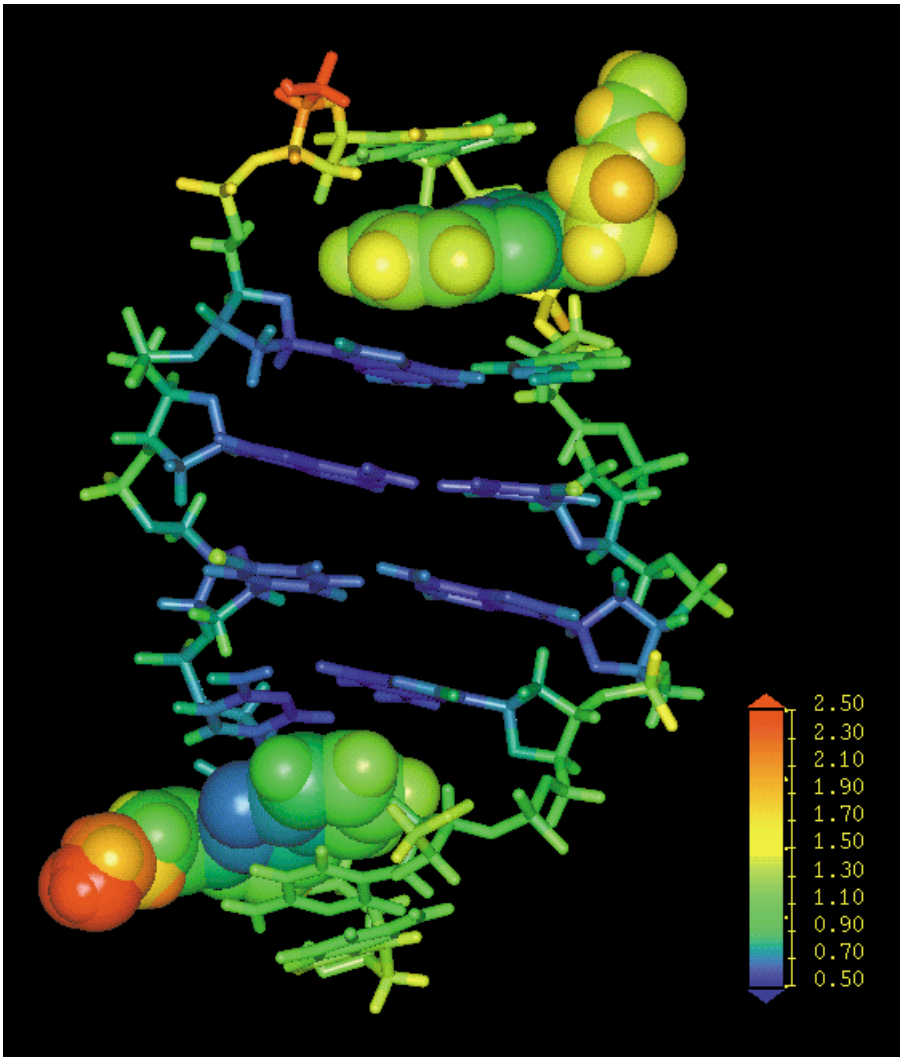

Fig. 7: Average structure of the complex between **1** and $d(CGATCG)_2$ over 100 ps MD following model II (see text). The colour range from blue to red reproduces the average root mean square deviations of the atoms from the average structure from 0.5 to 2.5 Å. (Water molecules and ions have been deleted for clarity)

lengths were used, providing different partition coefficients (1.3 (**1**)) and 2.38 (**2**)). It was found on a previous work [8] that **1** and **2** exhibit very different interactions with membranes: while the most hydrophobic**, [2],** due to micelle formation, exhibited only superficial interactions with the bilayers, **1** could incorporate the external layer of the membrane. As **1** was also more active *in vitro* against tumoral stems MCF7 and HL60 (unpublished), it was important to know if the mechanism involved was only due to enhanced membrane interactions.

The present study clearly shows that the two derivatives interact quite differently with $d(CGATCG)_2$: **2** exhibits weak interactions with $d(CGATCG)_2$, only evocative of an external binding at the level of the G1C6 bases and is weakly mutagenic. Therefore, **2** does not fulfill the requirements for a drug with good anticancer activity in agreement with the in vitro tests. The interactions of **1** with DNA are quite different. Both $d(CGATCG)_2$ proton and phosphorus chemical shift variations are suggestive of an intercalation of the aromatic part of the molecule at the level of the C1G2 bases. Furthermore, the symmetry of the oligonucleotide agrees with the 2 : 1 stoichiometry observed. The molecular dynamics study confirms a stable intercalation of **1** in between the CG bases of the DNA fragment. The fact that none of the models is able to satisfy all the distance restraints seen by NMR spectroscopy means that fast exchange must occur between different insertion schemes but an insertion of **1** in the major groove appears the most likely, although similar molecules were found to best intercalate in the minor groove [5].

Apart from the pyridopurin-like structure, that governs the specificity and also the overall intercalating properties, that is to say the basic anticancer activity, crucial activity enhancements can be obtained, depending on the amphiphilic properties conferred by the side chains. **[1]** exhibits intercalating properties and increased interactions with membranes. These properties both appear more or less directly linked to an easy diffusion in/between apolar medium (membrane and intra-DNA medium) and also the aqueous bulk. This is simply represented by a log(P) value of 1.3 and should be considered as a first rule for the syntheses to come. The strong intramolecular connectivity observed between the H2 proton of the third cycle, and H2′ proton of the terminal methylen group (satisfied in our proposed model (Fig. 7) reveals a rather packed conformation of the side chain, that could also enhance the interactions – stacking/intercalation – with the nucleic bases. This preference for a packed conformation of **1** is confirmed by our *ab-initio* calculations that reveal a minimum energy structure with a strong hydrogen bond between the terminal hydroxyl hydrogen and nitrogen N5. Moreover four cycle structures are well-known for their intercalation properties [5]. Therefore, the set-up of a "fourth ring" structure by negatively charging the terminal part of the two-carbon chain, (e.g. by using a carboxylic substituant and form $N_3{-}COO{-}$ bond) might result in a supplementary enhancement of activity.

4. Experimental

4.1. Synthesized components

4-(Pyrido[1,2-*e*]purin-4-ylamino)-1-butanol, (**1**) ^{1}H NMR, $CDCl_3$, (ppm), $\delta = 8.48$, H_2 (1 H, s); $\delta = 7.67$, H_6(1 H, d); $\delta = 7.52$, H_7(1 H, t); $\delta = 6.99$, H_8(1 H, t); $\delta = 8.63$, H_9(1 H, d); $\delta = 3.79$, $H_{1'}$(2 H, mr) ; $\delta = 1.89$, $H_{2'}$(2 H).; $\delta = 1.77$, $H_{3'}$(2 H); $\delta = 3.89$, $H_{4'}$(2 H, t). Log(P) = 1.34. typical linewidthes of 8 Hz(water) and 0.4 Hz($CHCl_3$).

6-(Pyrido[1,2-*e*]purin-4-ylamino)-1-hexanol, (**2**) ^{1}H NMR, $CDCl_3$, (ppm), $\delta = 8.48$, H_2 (1 H, s); $\delta = 7.67$, H_6(1H, d); $\delta = 7.51$, H_7(1 H, t); $\delta = 6.99$, H_8(1 H, t); $\delta = 8.63$, H_9(1 H,d); $\delta = 3.79$, $H_{1'}$(2 H, mr); $\delta = 1.89$, $H_{2'}$(2 H, mr); $\delta = 1.47$, $H_{3'}$, (2 H); $\delta = 1.41$, $H_{4'}$-$H_{5'}$(4 H, mr); $\delta = 3.60$, $H_{6'}$, (2 H). Log(P) = 2.38. typical linewidthes of 16 Hz(water) and 2 Hz ($CHCl_3$).

4.2. Materials

The self complementary hexamer $d(CGATCG)_2$ purchased by Institut Pasteur Paris, was used without further purification and dissolved in a buffer containing 160 mM KCl, 0.15 mM EDTA, 20 mM sodium phosphate at pH 7 in either pure D_2O or (for the observation of exchangeable protons) D_2O/H_2O 10/90. In the former case, the solution was lyophilized and resuspended in 99.98% D_2O and degassed before experiment.

4.3. Analytical methods

NMR spectra from ^{1}H NMR experiments were recorded on a AM400WB Bruker, and on a DRX-600 Bruker spectrometers. 1D spectra in D_2O were recorded at 277 K and 296 K using a linewidth of 4000 Hz and 32,000 complex points. A "jump-and-return" sequence [16] without water presaturation was used to observe exchangeable protons in H_2O/D_2O. NOESY spectra were obtained with the TPPI method [15] and 2048 points in both dimensions. Typical spectral width was 3800 Hz. Sinebell shifted filters were also used for Fourier transform in the two dimensions. Mixing time ranged from 70 ms (for estimation of nOe intensities) up to 0.7 s. Double Quantum filter COSY [17] and HOHAHA [18, 19] experiments (spin lock of 2,5 kHz) were also performed to confirm proton attribution as described in other works. ^{31}P NMR spectra were recorded on the same samples as those used for proton spectra using standard acquisition and composite pulse proton decoupling.

4.4. Molecular modeling

Following experimental results and due to the computational cost of the simulations, molecule **1**, only, was modeled inside the DNA hexamer duplex. The charges and geometry of **1** were optimized at the ab-initio RHF/6-31G* level of theory using GAMESS [20]. Partial charges were deduced from the calculation of the electrostatic potential following the CHELPG (Charges from ELectrostatic Potential Grid) algorithm with additional constraints to satisfy the total charge and dipole of the molecule.

All parameters for DNA and ions were taken from the CHARMM22 force field [21], and parameters for **1** (other than charges) come from the extended CHARMM/Quanta force field [22]. A rapid view at the nOes from NMR experiments suggests that **1** intercalates between C and G bases. We used initial structures obtained in a previous work [23] for our modeling study of molecule **1** inserted into d(CGATCG). Four intercalation schemes are possible, a priori:

I) **1** in the major groove with N5 atom facing C5-G6
II) **1** in the major groove with N5 atom facing C1-G2
III) **1** in the minor groove with N5 atom facing C1-G2
IV) **1** in the minor groove with N5 atom facing C5-G6

Molecule **1** was inserted "manually" following these 4 schemes with Insight. 10 potassium counterions were initially placed at the O−P−O bisector of each phosphate linking group, 3 Å away from the phosphorus atoms.

Starting from the above initial structures, energy minimizations and Molecular Dynamics (MD) simulations were run with CHARMM [22]. To avoid rapid exclusion of molecule **1** from DNA and/or rapid unwinding of this small portion of DNA double helix, several restraints were initially applied to the system: first, 3 kinds of distance restraints were introduced:

- between potassium ions and nearby phosphorus atoms to prevent escape of the ions with force constant KN1. (10 restraints)
- between acceptor and donor atoms of the Watson Crick base pairs involving cytosines and guanines at the extremities of the duplex to prevent DNA unwinding with force constant KN2. (12 restraints)
- finally, between proton atoms to satisfy the experimental nOes with force constant KN3 (13 restraints for each inclusion site according to Table 5 and excluding nOes obtained for 400 ms mixing time only.).

Heavy atoms of DNA and ions were first restrained to their original position with force constants KH1 = KH2 = 5.0 kcal/mol/Å^2 and distance restraint forces were set to KN1 = KN2 = 5.0 and KN3 = 2.0 kcal/mol/Å^2. Then, all systems were energy minimized to a final gradient of 0.01 kcal/mol/Å^2.

Starting from the minimized coordinates, 10 ps equilibration Langevin dynamics simulations at T = 300 K were run for each intercalation model with position restraints KH1 = 0.1 and KH2 = 2.0 kcal/mol/Å^2 for Heavy atoms of DNA and ions, respectively, and distance restraints unchanged: KN1 = KN2 = 5.0 and KN3 = 2.0 kcal/mol/Å^2. Then production MD simulations were run following protocols named a):

a) Starting from the strauctures obtained after the equilibration stage, 50 ps "restrained" MD steps after relieving restraints on the ions: KH1 = KN1 = 0 while maintaining all other restraints unchanged.

In a second, more realistic, stage of the modelling, DNA + **1** + 10 potassium ions, as obtained from the previously described "in vacuum" 0.01 kcal/mol/Å^2 final gradient minimization, were immersed into a 40 Å

side box of equilibrated water molecules. Waters with oxygen atoms closer than 2.5 Å from any non-water heavy atom (non H) were discarded. The total system consisted of 1954 water molecules and 6318 atoms. Periodic boundary conditions for nonbonded interactions were applied in all three dimensions for a cubic box of 40 Å side, with 12 Å cutoff. Particle mesh Ewald was used to compute electrostatic interactions. Then the exact same protocol of minimization and stage a) MD simulation as for the "in vacuum" case was used and followed by stage b) and c) below:

b) Starting from a), 100 ps "small restraint" MD steps with restraints on Watson Crick base pairs only with KN2 = 2.0 kcal/mol/Å^2.
c) Finally, starting from b), 50 ps "free" MD steps with all restraining forces set to zero.

References

1 N'Goy, K.; de-Meester, C.; Pairon, D.; Fabry, L.; Loukakou, B.; N'Zouzi; Saint-Ruf, G.; Mercier, M.; Poncelet, F.: Mutation Res. **136**, 23 (1984)
2 Tsuda, M.; Takayashi, Y.; Nagao, M.; Hirayama, T.; Sugimura, T.: Mutation Res. **78**, 331 (1980)
3 Debouzy, J. C.; Gueiffier, A.; Fauvelle, F.; Lhassani, M.; Kerbal, A.; Peinnequin, A.; Dejean, E.; Neirinck, V.; Bachelet, C.; Chapat, J. P.: Boll. Chim. Farm. **135**, 192 (1996)
4 Cardinaud, I.: Montpellier UFR Pharmaceutiques (1992)
5 Gueiffier, A.; Viols, H.; Chapat, J. P.; Chavignon, O.; Teulade, J. C.; Dauphin, G. J.: Heterocycl. Chem. **27**, 421 (1990)
6 Teulade, J. C.; Gueiffier, A.; Viols, H.; Chapat, J. P.; Grassy, G.; Perly, B. J.: Chem. Soc. Perkin. Trans I, 1895 (1989)
7 Pinguet, F.; Mavel, S.; Benakka, N.; Galtier, C.; Viols, H.; Gueiffier, A.: Eur. J. Med. Chem., in press
8 Dabouis, V.; Debouzy, J. C.; Gueiffier, A.; Crouzy, S.: Boll. Chim. Farm. **138**, 453 (1999)
9 Debouzy, J. C.; Gueiffier, A.; Dabouis, V.: Ann. Pharm. Fr. **56**, 197 (1998)
10 Delepierre, M.; Maroun, R.; Garbay-Jaureguiberry, C.; Igolen, J.; Roques, B. J.: Mol. Biol. **210**, 211 (1989)
11 Kaplan, J. I.; Fraenkel, G.: NMR of chemically exchanging systems. Academic Press Inc. New-York 1980
12 Feigon, J.; Denny, W. A.; Leupin, W.; Kearns, D. R.: J. Med. Chem. **27**, 450 (1984)
13 Job, P.: Ann. Chim. **9**, 113 (1928)
14 Gorenstein, D. G.: Phosphorus-31; Principles and applications. Pergamon, New-York 1984
15 Marion, D.; Wütrich, K.: Biochem. Biophys. Res. Comm. **113**, 967 (1983)
16 Plateau, P.; Guéron, M. J.: Am. Chem. Soc. **104**, 7310 (1982)
17 Kumar, A.; Ernst, R. R.; Wütrich, K.: Biochim. Biophys. Res. Comm. **95**, 1 (1980)
18 Bax, A.; Morris, G. J.: Magn. Res. **42**, 501 (1981)
19 Glore, G. M.; Gronenborn, A. M.: Embo. J. **2**, 2109 (1983)
20 Schmidt, W.; Baldridge, K. K.; Boatz, J. A.; Elbert, S. T.; Gordon, M. S.; Jensen, J. J.; Koseki, S.; Matsunaga, N.; Nguyen, K. A.; Su, S.; Windus, T. L.; Dupuis, M.; Montgomery, J. A.: Comput. Chem. 1347 (1993)
21 MacKerell, A. D. J.: J. Phys. Chem B. **102**, 586 (1998)
22 Brooks, B. R.; Bruccoleri, R. E.; Olafson, B. D.; States, D. J.; Swaminathan, S.; Karplus, M. J.: Comput. Chem. **4**, 187 (1983)
23 Debouzy, J. C.; Crouzy, S.; Dabouis, V.; Gueiffier, A.; Brasme, B.; Bachelet, C.; Favier, A.; Simorre, J. P.; Mazet, L.; Peinnequin, A.: Arch. Biochem. Biophys. **367**, 202 (1999)

Received May 22, 2000
Accepted June 20, 2000

J. C. Debouzy
Centre de Recherches du Service de Santé des Armées
Av. des maquis du Grésivaudan
38702-La Tronche cedex
France
jcdebouzy@compuserve.com